Robotica (2016) volume 34, pp. 2860–2877. © Cambridge University Press 2015
doi:10.1017/S0263574715000466

Task-space dynamics and motion/force control of fixed-base manipulators under reaction null-space-based redundancy resolution

Dragomir Nenchev*, Ryohei Okawa and Hiroki Sone

Graduate School of Engineering, Tokyo City University, Tamazutsumi 1-28-1, Setagaya-ku, Tokyo 158-8557, Japan

(Accepted May 20, 2015. First published online: June 17, 2015)

SUMMARY

This paper introduces a task-space dynamics formulation for fixed-base serial-link kinematically redundant manipulators and a motion/force controller based on it. The aim is to alleviate joint-space instability problems that have been observed with other motion/force controllers. The dynamics are represented in floating-base coordinates, wherein the end effector is regarded as the floating base. This representation gives rise to a momentum-conserving redundancy resolution scheme based on the reaction null-space (RNS) method used in past studies on free-floating and flexible-base space robots. A generalized inverse is obtained that is shown to satisfy the conditions for dynamic consistency in the sense of the operational space (OS) formulation, but may lead to the joint-space instabilities observed earlier. The proposed controller is based on the pseudoinverse of the coupling inertia matrix and ensures reactionless link motion that does not disturb the force balance at the end effector. The performance of the RNS motion/force controller is examined by comparison to that with an OS motion/force controller. It is shown that while the performance in task-space of both controllers is satisfactory, the joint-space performance of the proposed controller is superior.

1. Introduction

This work addresses the problem of motion/force control of redundant serial-link manipulators on a fixed base. A number of model-based controllers have been developed throughout the years with the help of task-space dynamic models. The adoption of such models is a fairly straightforward task when the manipulator is a non-redundant one. Representative pioneering works include refs. [1–4], a concise overview is given in ref. [5]. On the other hand, when the manipulator is a kinematically redundant one, it is known that a formulation based on task-space dynamics only would be insufficient. Indeed, joint-space dynamics cannot be neglected due to the inherent self-motion property; therefore, the null-space dynamics have to be involved in addition to the task-space ones. Early works that tackle this problem include the OS method,[4] the dynamic control algorithm,[6] the augmented impedance controller[7] and the compliant motion controller.[8] The main feature of the OS method is that task and null-space dynamics are completely decoupled through the so called "dynamically consistent relationship".[9,10] The latter two controllers are based on the extended task-space approach,[11] wherein kinematic redundancy is parametrized in a minimal way. The same approach was adapted to derive controllers with a dynamic decoupling property[12,13] and a compliance controller.[14] Impedance control was tackled under the dynamically consistent relationship in refs. [15–17].

Recently, an attempt was made to unify the derivation of a number of dynamic controllers within an optimal control framework, by assigning appropriate metrics for a cost function.[18] It was shown that while the controllers' performance in task space was quite satisfactory, in joint space very different behaviors were observed. In particular, algorithms involving a quadratic form that includes the inverse of the link inertia matrix, as in the underlying transform (or metric) under the OS formulation[1], exhibited problematic performance. Similar problems have been reported elsewhere.

* Corresponding author. E-mail: nenchev@ieee.org

[1] The inverse of the end-effector mobility tensor,[2,19] called also "operational space inertia matrix (OSIM)".[20]

https://doi.org/10.1017/S0263574715000466 Published online by Cambridge University Press

In ref. [8] the authors noticed that significant errors appeared in their impedance controller, and resorted therefore to manipulability maximization[21] within the null space of the primary task. In ref. [17], impedance control was experimentally evaluated with a seven-DOF manipulator (the DLR light-weight robot, generation II). It was concluded that dynamic decoupling is difficult to be realized in practice because the decoupling accuracy is limited due to ill-conditioning of the transform. In ref. [22], an overview of the state-of-the-art, OS control is presented. It was reconfirmed that stability can usually be demonstrated in task-space only. The joint-space instability problems were attributed to the null-space dynamics, which is in accordance with the results that have been previously reported, e.g. in ref. [8]

From this brief overview, we can conclude that the joint-space behavior of redundant manipulators exhibiting satisfactory performance in task space under motion/force or impedance control, is not fully understood yet. One of the reasons for the undesirable behavior seems to be the ill-conditioning of the underlying transform/metric. As another reason, joint velocity build-up can be pointed out, e.g. as observed in early works on task-space dynamic control of kinematically redundant manipulators under torque minimization.[23,24] The problem can be related to the lack of integrability of joint acceleration, thus yielding a second-order non-holonomic behavior of the manipulator, similar to that discussed in ref. [25] for free-joint manipulators. Analysis has been provided in refs. [26,27] but nevertheless, the problem is still actual as also apparent from more recent results in refs. [28–31].

The aim of this work is to design a task-space motion/force controller capable to alleviate the joint-space instability problem, without necessarily resorting to null-space control. First, we introduce a new formulation that, similarly to the OS formulation, is shown to yield a dynamically consistent relationship. The dynamic model is derived w.r.t. a moving coordinate frame attached to the end effector. Force components facilitating motion/force control, i.e. the force of constraint and the inertial force due to end-effector acceleration, can then be obtained in explicit form, without involving any transformation from the joint space. Furthermore, an additional force component stemming from the inertial coupling between the end effector and the rest of the links is explicitly visible. This component gives rise to a joint-space decomposition scheme wherein integrability of the joint acceleration can be ensured with generalized momentum conservation, under certain assumptions. Also, the ill-conditioning problem can be alleviated by avoiding quadratic forms that include the inverse of the link inertia matrix. Further on, we will show that the null-space solution component yields reactionless motion, i.e. motions of the intermittent links that do not impose any force/moment on the end effector. This property can be regarded as a necessary condition for complete dynamic decoupling between the particular and null-space solution components. Finally, we will show that the proposed controller minimizes part of the kinetic energy stemming from the inertial coupling. This, in conjunction with momentum conservation, leads to a motion with low kinetic energy.

The decomposition scheme outlined above is based on the RNS method[32,33] used so far to ensure the dynamic decoupling between an unfixed base (e.g. that of a free-floating[34] or a flexible-base robot[35,36]) and the rest of the links. We will first reformulate the original RNS notation, w.r.t. end-effector dynamic decoupling. Such reformulation can be done in a straightforward manner, as shown in ref. [37] for a free-floating space robot, and in ref. [38] for a quasi-flexible base robot. Then, we will show how to implement the new notation in motion/force control task scenarios with a fixed-base serial-link kinematically redundant manipulator. Finally, results of a comparison to motion/force control under the OS formulation will be presented to evaluate the performance of the new scheme.

The remainder of this article is organized as follows. Section 2 introduces background and notations. End-effector dynamics derived via the floating-base representation and the respective inverse dynamics solution obtained through RNS decomposition is described in Section 3. In Section 4, the momentum conserving RNS motion/force controller is introduced. In Section 5, RNS controller performance is compared with that of an OS controller. The last section gives the conclusions.

2. Background and Notation

The dynamics of a redundant serial-link robot manipulator in end-effector coordinates have been described within the OS formulation[4,9] as

$$\boldsymbol{M}_e(\boldsymbol{\theta})\dot{\mathcal{V}} + \mathcal{C}_e(\boldsymbol{\theta}, \dot{\boldsymbol{\theta}}) + \mathcal{G}_e(\boldsymbol{\theta}) = \mathcal{F}. \tag{1}$$

https://doi.org/10.1017/S0263574715000466 Published online by Cambridge University Press

$\boldsymbol{\theta} \in \Re^n$ denotes the joint coordinate vector, $\mathcal{V}, \mathcal{F} \in \Re^m$ denote end-effector velocity and force, $\mathcal{C}_e(\boldsymbol{\theta}, \dot{\boldsymbol{\theta}})$, $\mathcal{G}_e(\boldsymbol{\theta})$ stand for Coriolis and centrifugal force and gravity force, respectively. Matrix $\boldsymbol{M}_e(\boldsymbol{\theta})$ is called the 'OSIM[20] and is represented as the inverse of the end-effector *mobility tensor*:[2,19]

$$\boldsymbol{M}_e(\boldsymbol{\theta}) = \left(\boldsymbol{J}(\boldsymbol{\theta})\boldsymbol{M}_l^{-1}(\boldsymbol{\theta})\boldsymbol{J}^T(\boldsymbol{\theta})\right)^{-1} \in \Re^{m\times m}, \tag{2}$$

where $\boldsymbol{J}(\boldsymbol{\theta}) \in \Re^{m\times n}$ stands for the manipulator Jacobian. It should be noted that the manipulator dynamics in end-effector coordinates (1) have been obtained from the equation of motion in joint coordinates:

$$\boldsymbol{M}_l(\boldsymbol{\theta})\ddot{\boldsymbol{\theta}} + \boldsymbol{c}_l(\boldsymbol{\theta}, \dot{\boldsymbol{\theta}}) + \boldsymbol{g}_l(\boldsymbol{\theta}) = \boldsymbol{\tau}, \tag{3}$$

via the (transposed) inertia-weighted generalized inverse

$$\boldsymbol{J}_M^{\#}(\boldsymbol{\theta}) = \boldsymbol{M}_l^{-1}(\boldsymbol{\theta})\boldsymbol{J}^T(\boldsymbol{\theta})\boldsymbol{M}_e(\boldsymbol{\theta}).$$

$\boldsymbol{\tau} \in \Re^n$ is the joint torque, $\boldsymbol{M}_l(\boldsymbol{\theta}) \in \Re^{n\times n}$ stands for the link inertia matrix, $\boldsymbol{c}_l(\boldsymbol{\theta}, \dot{\boldsymbol{\theta}})$, $\boldsymbol{g}_l(\boldsymbol{\theta}) \in \Re^n$ denote Coriolis and centrifugal force and gravity force vectors, respectively. Note that the end effector is not in contact with the environment and therefore, $\mathcal{F}$ is not an external force: $\mathcal{F} = \boldsymbol{J}_M^{\#T}\boldsymbol{\tau}$. Since this force depends on the particular choice of a generalized inverse, the dynamics representation (1) is not unique.

Consider now a motion/force control scenario wherein the end effector is partially constrained by the environment. The end-effector dynamics become[4]

$$\mathcal{F} - \boldsymbol{M}_e(\boldsymbol{\theta})\dot{\mathcal{V}} - \mathcal{C}_e(\boldsymbol{\theta}, \dot{\boldsymbol{\theta}}) - \mathcal{G}_e(\boldsymbol{\theta}) = \mathcal{F}_\kappa, \tag{4}$$

where $\mathcal{F}_\kappa$ is the contact force imposed on the end effector from the environment. To meet the control objective, a reference end-effector force is designed as

$$\begin{aligned} \mathcal{F}^{ref} &= \mathcal{F}_m^{ref} + \mathcal{F}_\kappa^{ref}, \\ \mathcal{F}_m^{ref} &= \boldsymbol{M}_e(\boldsymbol{\theta})\boldsymbol{S}\dot{\mathcal{V}}^{ref} + \mathcal{C}_e(\boldsymbol{\theta}, \dot{\boldsymbol{\theta}}) + \mathcal{G}_e(\boldsymbol{\theta}) + \boldsymbol{M}_e(\boldsymbol{\theta})\dot{\boldsymbol{S}}\mathcal{V}, \\ \mathcal{F}_\kappa^{ref} &= \boldsymbol{S}^{\perp}\mathcal{F}_c^{ref}, \end{aligned} \tag{5}$$

where $\mathcal{F}_m^{ref}$ and $\mathcal{F}_\kappa^{ref}$ are two components referring to end-effector motion and contact force, respectively. $\boldsymbol{S}$ is a selection matrix suitably defined to specify the unconstrained (motion) directions, while $\boldsymbol{S}^{\perp}$ is its complement. $\dot{\mathcal{V}}^{ref}$ and $\mathcal{F}_c^{ref}$ are reference values for the motion and force tasks, respectively, that usually involve feedback control terms.

Further on, since the manipulator is redundant, there is an infinite set of control joint torques that could be applied without affecting the resultant forces at the end effector:[4,9]

$$\boldsymbol{\tau} = \boldsymbol{J}^T\mathcal{F}^{ref} + \left(\boldsymbol{I} - \boldsymbol{J}^T\boldsymbol{J}_M^{\#T}\right)\boldsymbol{\tau}_a, \tag{6}$$

where $(\boldsymbol{I} - \boldsymbol{J}^T\boldsymbol{J}_M^{\#T})$ denotes a projector onto the null space of the transposed inertia-weighted generalized inverse of the Jacobian, $\boldsymbol{I}$ standing for the $n \times n$ identity matrix. $\boldsymbol{\tau}_a$, an arbitrary joint torque vector, parametrizes (in a non-minimal way) the set of joint torques that do not impose any end effector force. Moreover, as noted in ref. [10] there is also another infinite set of control joint torques that produce the same end-effector acceleration as a given end-effector force:

$$\boldsymbol{\tau} = \boldsymbol{M}_l\boldsymbol{J}^{\#}\boldsymbol{M}_e^{-1}\mathcal{F}^{ref} + \boldsymbol{M}_l\left(\boldsymbol{I} - \boldsymbol{J}^{\#}\boldsymbol{J}\right)\boldsymbol{\theta}_a, \tag{7}$$

where $\boldsymbol{\theta}_a$ stands for an arbitrary joint acceleration vector. The two joint-torque sets (6) and (7) are compatible (or dynamically consistent), only when the inertia-weighted generalized inverse of the Jacobian is applied in (7). This leads to *complete dynamic decoupling* between the particular

https://doi.org/10.1017/S0263574715000466 Published online by Cambridge University Press

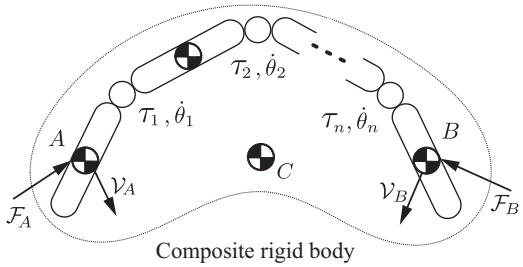


Fig. 1. Model of a free-floating serial-link manipulator. With joints locked momentarily, the manipulator can be regarded as a composite rigid body (CRB). Points A and B are characteristic points on the two end-links, point C denoting the total CoM.

components responsible for the motion/force control task and the null-space components. It was shown in ref. [10] that the following four conditions will be then satisfied:

$$\mathcal{T}_n = \boldsymbol{M}_l \mathcal{Q}_n, \quad \mathcal{T}_p = \boldsymbol{M}_l \mathcal{Q}_p \tag{8}$$

and

$$\mathcal{T}_n \perp \mathcal{Q}_p, \quad \mathcal{T}_p \perp \mathcal{Q}_n, \tag{9}$$

where $\mathcal{Q}$ and $\mathcal{T}$ denote the joint motion (velocity/acceleration) and its dual (momentum/force) subspace, while subscripts "p" and "n" stand for components from the row and null subspaces of the underlying transform.

The property of complete dynamic decoupling plays an important role in motion/force and impedance control design, since task and null-space control components can be designed independently. As noted in the Introduction, though, the nominal behavior in joint space determined by the task-space control component may become unstable due to ill-conditioning of the end-effector mobility tensor and the respective metric. Also, the joint velocity may grow in an uncontrollable fashion because of the non-integrability of joint acceleration. Although these problems can be alleviated via the null-space control component, it would be much more desirable to have a controller with a satisfactory nominal behavior.

3. End-Link Dynamics with Floating-Base Coordinates

In this section, we show how the dynamics of a fixed-base manipulator can be rewritten by adopting a floating-base dynamic model. The special properties of this model are then highlighted and shown to be useful in the design of a motion/force controller with the desirable nominal behavior.

3.1. Dynamics of a floating-base serial-link manipulator

Consider a free-floating serial-link manipulator with $n + 1$ links, as shown in Fig. 1. The two end-links are denoted as A and B. Without loss of generality, in what follows end-link A will be designated as the root link. It is convenient to assume that the root link is connected to the inertial frame via a virtual six-DOF joint. Hence, there are $n + 6$ generalized coordinates: the n joint coordinates plus the six coordinates of the root end-link. There are three points of interest: characteristic points on each of the two end-links (points A and B in Fig. 1) and the total center of mass (CoM point C). External spatial forces $\mathcal{F}_A$ and $\mathcal{F}_B$ act at points A and B, respectively. The motion of the two end-links is characterized by spatial velocities $\mathcal{V}_A$ and $\mathcal{V}_B$.

The system dynamics are described by two coupled equations:

$$\boldsymbol{M}_A \dot{\mathcal{V}}_A + \boldsymbol{M}_{Al} \ddot{\boldsymbol{\theta}} + \mathcal{C}_A + \mathcal{G}_A = \mathcal{F}_A + \boldsymbol{T} \mathcal{F}_B \tag{10}$$

and

$$\boldsymbol{M}_{Al}^T \dot{\mathcal{V}}_A + \boldsymbol{M}_l \ddot{\boldsymbol{\theta}} + \boldsymbol{c}_l + \boldsymbol{g}_l = \boldsymbol{\tau} + \boldsymbol{J}^T \mathcal{F}_B. \tag{11}$$

https://doi.org/10.1017/S0263574715000466 Published online by Cambridge University Press

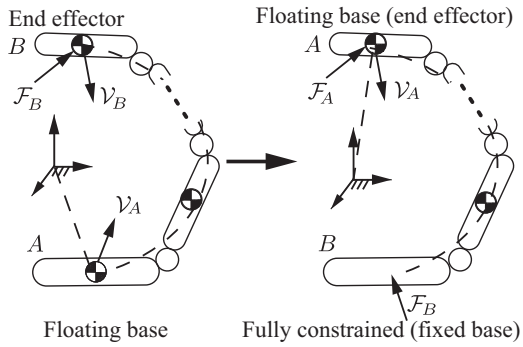


Fig. 2. In the floating-base manipulator model (the figure on the left) link A is the floating base (root link) while link B is the end effector. The fixed-base manipulator model is obtained when link A is assigned the role of the end effector (floating base, root link), while link B is being fully constrained to obtain the fixed base.

First, note that in (10) there are two linear force components. $\boldsymbol{M}_{Al}\ddot{\boldsymbol{\theta}}$ reflects the inertial coupling between end-link A and the rest of the links. $\boldsymbol{M}_{Al} \in \Re^{6\times n}$ will be referred to as the coupling inertia matrix.[32] Component $\boldsymbol{M}_A\dot{\mathcal{V}}_A$, on the other hand, represents the inertia force of the composite rigid body (CRB) obtained when the joints are momentarily locked. The CRB dynamics are characterized by the inertial properties of the entire system; they are represented in terms of end-link A coordinates. $\boldsymbol{M}_A \in \Re^{6\times 6}$, $\mathcal{C}_A$, $\mathcal{G}_A \in \Re^6$ denote CRB inertia matrix, non-linear coupling and gravity forces, respectively. $\boldsymbol{T} \in \Re^{6\times 6}$ is a spatial force transform.

Next, note that (11) would represent the dynamics of a "conventional" fixed-base manipulator, when link A is fixed. This manipulator is composed of all bodies except link A; because end-link A is the root, quantities $\boldsymbol{M}_l$, $\boldsymbol{c}_l$, $\boldsymbol{g}_l$ and $\boldsymbol{J}$ are those of the fixed-base manipulator, link B being its end effector. To adapt this floating-base notation to a fixed-base manipulator, we will keep end-link A as the root link, but designate it as the end effector. End-link B, on the other hand, will be fully constrained to become the fixed base. This implies the renumbering of joints and links in reverse order, as illustrated in Fig. 2.

3.2. Properties of system dynamics

The partial dynamics (10) have some desirable properties from the viewpoint of motion/force controller design. These properties will be examined below via some idealizing assumptions. First, note that end-effector acceleration $\dot{\mathcal{V}}_A$ and (external) force $\mathcal{F}_A$ are explicitly present in the equation. Hence, there is no need to involve a coordinate transformation, such as the transposed inertia-weighted generalized inverse. Furthermore, note the presence of the term $\boldsymbol{M}_{Al}\ddot{\boldsymbol{\theta}}$; it accounts for the joint-space dynamics. This is in contrast to the OS dynamics representation (1) wherein the joint-space dynamics remain completely hidden.

Assume now that the system is under zero gravity or static balance ($\mathcal{G}_A = \boldsymbol{T}\mathcal{F}_B$) and the joints are locked. Then, from (10) we obtain the CRB dynamic relationship:

$$\mathcal{F}_A = \boldsymbol{M}_A\dot{\mathcal{V}}_A. \tag{12}$$

Next, assume a stationary or uniformly moving end effector ($\dot{\mathcal{V}}_A = 0$). When the manipulator accelerates, the end-effector will be subjected to the spatial force:

$$\mathcal{F} = \boldsymbol{M}_{Al}\ddot{\boldsymbol{\theta}}. \tag{13}$$

Further on, we focus on the partial dynamics (11). Assume again zero gravity or a stationary state. When a joint torque is applied, the joints accelerate as follows:

$$\ddot{\boldsymbol{\theta}} = \boldsymbol{M}_l^{-1}\boldsymbol{\tau}. \tag{14}$$

https://doi.org/10.1017/S0263574715000466 Published online by Cambridge University Press

On the other hand, when the end effector accelerates, then the respective joint torque is

$$\boldsymbol{\tau} = \boldsymbol{M}_{Al}^T \dot{\mathcal{V}}_A. \tag{15}$$

With the help of (13)–(15), and under force balance $\mathcal{F}_A = \mathcal{F}$, the end-effector force/acceleration relation (12) can be expressed as

$$\mathcal{F}_A = \boldsymbol{M}_{Al} \boldsymbol{M}_l^{-1} \boldsymbol{M}_{Al}^T \dot{\mathcal{V}}_A. \tag{16}$$

By comparison to (12), it becomes apparent that the CRB inertia matrix can be represented as

$$\boldsymbol{M}_A = \boldsymbol{M}_{Al} \boldsymbol{M}_l^{-1} \boldsymbol{M}_{Al}^T. \tag{17}$$

This matrix can be regarded as an equivalent of the OSIM.

3.2.1. Reactionless motion property. Assume again that end-effector force $\mathcal{F}_A$ is the only acting external force (e.g. under static balance or zero-gravity condition). The joint acceleration obtained from (10) is

$$\ddot{\boldsymbol{\theta}} = \boldsymbol{M}_{Al}^{\#} \mathcal{F}_A + (\boldsymbol{I} - \boldsymbol{M}_{Al}^{\#} \boldsymbol{M}_{Al}) \ddot{\boldsymbol{\theta}}_a, \tag{18}$$

where $\boldsymbol{M}_{Al}^{\#}$ denotes a generalized inverse of the coupling inertia matrix. The second term on the r.h.s. is a vector from the null space of this matrix, $\ddot{\boldsymbol{\theta}}_a$ denoting an arbitrary joint acceleration. This term appears since we deal with a redundant manipulator ($n > 6$). Hence, there is an infinite set of joint accelerations that do not alter the force balance at the end-effector:

$$\{\ddot{\boldsymbol{\theta}}_{RL} : \ddot{\boldsymbol{\theta}} = (\boldsymbol{I} - \boldsymbol{M}_{Al}^{\#} \boldsymbol{M}_{Al}) \ddot{\boldsymbol{\theta}}_a, \forall \ddot{\boldsymbol{\theta}}_a \in \Re^n\}.$$

Any acceleration from the above set can be characterized as *reactionless*. The null space of the coupling inertia matrix $\boldsymbol{M}_{Al}$ plays an important role in the following derivations. We will henceforth refer to this null space as the *end-effector reaction null space* (EE-RNS).

3.2.2. Integrability property. The necessary and sufficient conditions for integrability are given below.

Proposition 1 (necessary condition for integrability). *Assume quasi-static force balance ($\mathcal{G}_A = \mathcal{F}_A + \boldsymbol{T}\mathcal{F}_B$) and a non-linear force represented as $\mathcal{C}_A \approx \dot{\boldsymbol{M}}_A \mathcal{V}_A + \dot{\boldsymbol{M}}_{Al} \dot{\boldsymbol{\theta}}$. Then, the partial dynamics (10) can be integrated.*

Proof. Follows by direct substitution of the assumptions into (10). □

The integration results in the following constant of motion:

$$\boldsymbol{M}_A \mathcal{V}_A + \boldsymbol{M}_{Al} \dot{\boldsymbol{\theta}} = \boldsymbol{0}, \tag{19}$$

whereby the integration constant is assumed null. This relation can be interpreted as a momentum conservation constraint. Solving for the joint velocity, we obtain

$$\dot{\boldsymbol{\theta}} = -\boldsymbol{M}_{Al}^{\#} \boldsymbol{M}_A \mathcal{V}_A + \dot{\boldsymbol{\theta}}_{RL}, \tag{20}$$

where

$$\{\dot{\boldsymbol{\theta}}_{RL} : \dot{\boldsymbol{\theta}} = (\boldsymbol{I} - \boldsymbol{M}_{Al}^{\#} \boldsymbol{M}_{Al}) \dot{\boldsymbol{\theta}}_a, \forall \dot{\boldsymbol{\theta}}_a \in \Re^n\}$$

is an infinite set of joint velocities, referred to as *reactionless*, $\dot{\boldsymbol{\theta}}_a$ denoting an arbitrary joint velocity.

https://doi.org/10.1017/S0263574715000466 Published online by Cambridge University Press

Proposition 2 (sufficient condition for integrability). *For any $\boldsymbol{M}_{Al}^{\#}$, the necessary condition for integrability (19) should be enforced with the unique joint velocity $\dot{\boldsymbol{\theta}} = -\boldsymbol{M}_{Al}^{\#}\boldsymbol{M}_A\mathcal{V}_A$.*

Proof. Given a joint acceleration $\ddot{\boldsymbol{\theta}}(t)$, its integral is represented by an unique joint velocity vector, invariant w.r.t. a linear shift in the origin. The statement in the proposition implies that the reactionless joint velocity must be identically zero. Assuming the opposite ($\dot{\boldsymbol{\theta}}_{RL} \neq 0$), and noting that $\{\dot{\boldsymbol{\theta}}_{RL}\}$ is an infinite set parametrized by $\dot{\boldsymbol{\theta}}_a$, we arrive at the contradiction that there is more than one joint velocity for a given joint acceleration. Therefore, the reactionless velocity should be null. □

Henceforth, based on reasons to be outlined below, we resort to the Moore–Penrose-generalized inverse (pseudoinverse) in the equations.

Corollary 1. *Assume $\boldsymbol{M}_{Al}^{\#} \equiv \boldsymbol{M}_{Al}^{+}$. Then, to enforce integrability, the following reactionless joint acceleration must be employed:*

$$\begin{aligned}\ddot{\boldsymbol{\theta}}_{RL} &= -\left(\boldsymbol{I} - \boldsymbol{M}_{Al}^{+}\boldsymbol{M}_{Al}\right)\dot{\boldsymbol{M}}_{Al}^{T}(\boldsymbol{M}_{Al}\boldsymbol{M}_{Al}^{T})^{-1}\boldsymbol{M}_A\mathcal{V}_A \\ &= \left(\boldsymbol{I} - \boldsymbol{M}_{Al}^{+}\boldsymbol{M}_{Al}\right)\dot{\boldsymbol{M}}_{Al}^{T}(\boldsymbol{M}_{Al}\boldsymbol{M}_{Al}^{T})^{-1}\boldsymbol{M}_{Al}\dot{\boldsymbol{\theta}},\end{aligned} \tag{21}$$

where $\boldsymbol{M}_{Al}^{+}$ denotes the pseudoinverse and $\dot{\boldsymbol{M}}_{Al} \equiv \frac{\mathrm{d}}{\mathrm{d}t}\boldsymbol{M}_{Al}$.

Proof. In (20), substitute $\boldsymbol{M}_{Al}^{\#}$ by $\boldsymbol{M}_{Al}^{+}$ and differentiate w.r.t. time under the sufficient condition $\dot{\boldsymbol{\theta}}_{RL} = \boldsymbol{0}$. Taking into account constraint (19), it is straightforward to arrive at (21). □

3.2.3. Dynamically consistent relationship. With the help of the EE-RNS, we can derive an infinite set of joint torque vectors that produce the same end-effector acceleration as a given end-effector force:

$$\boldsymbol{\tau} = \boldsymbol{M}_l\boldsymbol{M}_{Al}^{\#}\boldsymbol{M}_A\dot{\mathcal{V}}_A + \boldsymbol{\tau}_{RL}, \tag{22}$$

where

$$\{\boldsymbol{\tau}_{RL} : \boldsymbol{\tau} = \boldsymbol{M}_l(\boldsymbol{I} - \boldsymbol{M}_{Al}^{\#}\boldsymbol{M}_{Al})\ddot{\boldsymbol{\theta}}_a,\ \forall\ddot{\boldsymbol{\theta}}_a \in \Re^n\}. \tag{23}$$

Equation (22) was obtained by substituting (18) into (11), and ignoring the non-linear, gravity and reaction forces.

Proposition 3. *Generalized inverse*

$$\overline{\boldsymbol{M}}_{Al} = \boldsymbol{M}_l^{-1}\boldsymbol{M}_{Al}^{T}\left(\boldsymbol{M}_{Al}\boldsymbol{M}_l^{-1}\boldsymbol{M}_{Al}^{T}\right)^{-1}, \tag{24}$$

is a dynamically-consistent generalized inverse.

Proof. First, it can be confirmed by direct observation that for any $\boldsymbol{M}_{Al}^{\#}$, (22) together with (23) satisfies the two conditions (8). Next, we focus on the enforcement of the orthogonality conditions (9). To this end, observe that there is an infinite set of joint torques that do not alter the state of the end effector:

$$\boldsymbol{\tau} = \boldsymbol{M}_{Al}^{T}\dot{\mathcal{V}}_A + \left(\boldsymbol{I} - \boldsymbol{M}_{Al}^{T}\boldsymbol{M}_{Al}^{T^{\#}}\right)\boldsymbol{\tau}_a. \tag{25}$$

The second term on the r.h.s. is a null-space vector, $\boldsymbol{\tau}_a$ denoting an arbitrary joint torque vector. It is straightforward to confirm that for any $\boldsymbol{M}_{Al}^{\#}$, (25) satisfies (9). The unique generalized inverse that satisfies both, (8) and (9), is the dynamically-consistent generalized inverse $\overline{\boldsymbol{M}}_{Al}$. □

https://doi.org/10.1017/S0263574715000466 Published online by Cambridge University Press

It is worth noting that, when $\overline{\boldsymbol{M}}_{Al}$ is substituted into (23) and (25), the two null-space projectors will be related via a similarity transform[2]:

$$(\boldsymbol{I} - \overline{\boldsymbol{M}}_{Al}\boldsymbol{M}_{Al}) = \boldsymbol{M}_l^{-1}\big(\boldsymbol{I} - \boldsymbol{M}_{Al}^T\overline{\boldsymbol{M}}_{Al}^T\big)\boldsymbol{M}_l. \tag{26}$$

3.2.4. Coupling energy minimization. The dynamically consistent force/torque relationship derived above via generalized inverse $\overline{\boldsymbol{M}}_{Al}$, includes the inverse of the link inertia matrix (cf. (24)). As explained in the Introduction, this type of generalized inverses lead to ill-conditioning problems, such as error amplification,[18] and may induce joint-space instability. To avoid such problems, henceforth we employ the pseudoinverse as a generalized inverse. The complete dynamic decoupling property will then be sacrificed to guarantee joint-space stability, without involving the null-space component. The reactionless motion property, that guarantees conditions (8) of the dynamically consistent relationship via (22) and (23), though, will be unaffected.

The reason why we prefer the pseudoinverse will be explained in what follows. Consider first the total kinetic energy:

$$\begin{aligned} T = &\frac{1}{2}\big(m_A\boldsymbol{v}_A^T\boldsymbol{v}_A + \boldsymbol{\omega}_A^T\boldsymbol{I}_A\boldsymbol{\omega}_A\big) \\ &+ \frac{1}{2}\sum_{i=1}^{n-1}\big(m_i\boldsymbol{v}_i^T\boldsymbol{v}_i + \boldsymbol{\omega}_i^T\boldsymbol{I}_i\boldsymbol{\omega}_i\big) \\ &+ \frac{1}{2}\big(m_B\boldsymbol{v}_B^T\boldsymbol{v}_B + \boldsymbol{\omega}_B^T\boldsymbol{I}_B\boldsymbol{\omega}_B\big), \end{aligned} \tag{27}$$

where $m_{(\circ)}$, $\boldsymbol{I}_{(\circ)}$, $\boldsymbol{v}_{(\circ)}$, $\boldsymbol{\omega}_{(\circ)}$ denote mass, inertia tensor, CoM velocity and angular velocity of each link, respectively. Rewrite in a compact form as

$$T = \frac{1}{2}\mathcal{V}_A^T\boldsymbol{M}_A\mathcal{V}_A + \frac{1}{2}\dot{\boldsymbol{\theta}}^T\boldsymbol{M}_l\dot{\boldsymbol{\theta}} + \mathcal{V}_A^T\boldsymbol{M}_{Al}\dot{\boldsymbol{\theta}}. \tag{28}$$

The first two terms denote the kinetic energies of the CRB and of the links, respectively. The last term, referred to as the *coupling kinetic energy*, stands for the energy exchanged between the end effector and the rest of the links.

The coupling kinetic energy plays an important role in the derivations. To gain further insight, consider again a system under quasi-static force equilibrium, s.t. $\mathcal{G}_A = \mathcal{F}_A + \boldsymbol{T}\mathcal{F}_B$, or equivalently, a system in zero-gravity environment and no external forces. These special cases allow us to focus on the dynamics of link motion and the inertia coupling property. As clarified in the previous section, generalized momentum will then be conserved. The joint velocity, obtained from the particular component in (20) is

$$\dot{\boldsymbol{\theta}} = -\boldsymbol{M}_{Al}^{\#}\boldsymbol{M}_A\mathcal{V}_A. \tag{29}$$

With this velocity, the coupling kinetic energy becomes

$$\begin{aligned} T_{CE} &= -\mathcal{V}_A^T\boldsymbol{M}_A\mathcal{V}_A \\ &= -\dot{\boldsymbol{\theta}}^T\left(\boldsymbol{M}_{Al}^T\boldsymbol{M}_A^{-1}\boldsymbol{M}_{Al}\right)\dot{\boldsymbol{\theta}}, \end{aligned} \tag{30}$$

where the property $\boldsymbol{M}_{Al}\boldsymbol{M}_{Al}^{\#} = \boldsymbol{I}$ was used.

Next, note that to minimize (locally) the total kinetic energy under momentum conservation, it would be sufficient to minimize the partial kinetic energy, e.g. the coupling kinetic energy. For a given

[2] This is also true for the two null-space projectors in the OS formulation:
$(I - J_M^{\#}J) = M_l^{-1}(I - J^T J_M^{T^{\#}})M_l$.

https://doi.org/10.1017/S0263574715000466 Published online by Cambridge University Press

system configuration, this energy will be minimized iff the joint velocity norm is minimal. Such joint velocity can be obtained by choosing the pseudoinverse $\boldsymbol{M}_{Al}^{+}$ as a generalized inverse in (29).

With the above expression for the coupling kinetic energy, the system kinetic energy can be rewritten as

$$\begin{aligned} T &= \frac{1}{2}\dot{\boldsymbol{\theta}}^T \boldsymbol{M}_l \dot{\boldsymbol{\theta}} - \frac{1}{2}\mathcal{V}_A^T \boldsymbol{M}_A \mathcal{V}_A \\ &= \frac{1}{2}\dot{\boldsymbol{\theta}}^T \left(\boldsymbol{M}_l - \boldsymbol{M}_{Al}^T \boldsymbol{M}_A^{-1} \boldsymbol{M}_{Al}\right) \dot{\boldsymbol{\theta}}. \end{aligned} \tag{31}$$

The momentum conservation condition means that pausing the end-effector motion will necessarily lead to pausing link motion (under null initial momentum). Thus, the non-integrability (joint velocity build-up) problem, inherent to other task-space dynamic controllers, can be avoided.

4. Reaction Null-Space-Based Motion/Force Control

Our goal is to design a controller with a task-space control component that can ensure the desirable nominal behavior in joint space, such that large joint-velocity peaks and velocity build-up can be avoided. As shown in the previous section, the pseudoinverse of the coupling inertia matrix is worth being considered in the underlying redundancy resolution scheme. When deriving the relations, the idealizing assumptions from the previous section will be dropped and the complete dynamics (10) and (11) will be taken under consideration.

The derivation is based on the hybrid motion/force control approach presented in ref. [5], Chapter 7. End-effector A contacts the environment under a motion/force task scenario, being thereby constrained along $k < 6$ directions. This can be expressed via the equation $\boldsymbol{J}_\kappa(\boldsymbol{q})\dot{\boldsymbol{q}} = \boldsymbol{0}$, $\boldsymbol{J}_\kappa(\boldsymbol{q}) \in \Re^{k\times(6+n)}$ denoting the constraint Jacobian containing partial derivatives related to the environment constraint $\boldsymbol{\kappa}(\boldsymbol{q}) = \text{const}$. End-effector A's spatial force is then $\mathcal{F}_A = \boldsymbol{J}_{\kappa A}^T \boldsymbol{\lambda}$, where $\boldsymbol{\lambda} \in \Re^k$ is the Lagrange multiplier for the forces of constraint and $\boldsymbol{J}_{\kappa A}(\boldsymbol{q}) \in \Re^{k\times 6}$ is a submatrix of the constraint Jacobian s.t. $\boldsymbol{J}_{\kappa A}\mathcal{V}_A = \boldsymbol{0}$. Further on, denote $\mathcal{V}_A \equiv \boldsymbol{S}_v \boldsymbol{v}$ where $\boldsymbol{v} \in \Re^{6-k}$ is end-effector A's velocity along the unconstrained directions and $\boldsymbol{S}_v(\boldsymbol{q}) \in \Re^{6\times(6-k)}$ is defined from $\boldsymbol{S}_f^T \boldsymbol{S}_v = \boldsymbol{0}$, $\boldsymbol{S}_f(\boldsymbol{q}) \equiv \boldsymbol{J}_{\kappa A}^T(\boldsymbol{q})$.

Using (10), we first obtain the reference joint acceleration for the task-space (particular-solution) control component:

$$\begin{aligned} \ddot{\boldsymbol{\theta}}_p^{ref} &= \boldsymbol{M}_{Al}^{+}\left(\boldsymbol{S}_f \boldsymbol{f}_\lambda - \boldsymbol{M}_A \boldsymbol{S}_v \boldsymbol{\alpha}_v - \boldsymbol{M}_A \dot{\boldsymbol{S}}_v \boldsymbol{v}\right) \\ &\quad + \boldsymbol{M}_{Al}^{+}\left(\boldsymbol{T}\mathcal{F}_B - \mathcal{C}_A - \mathcal{G}_A\right). \end{aligned} \tag{32}$$

As shown in the Appendix, this control acceleration ensures complete decoupling between the motion and force subtasks for the closed-loop system, s.t. $\dot{\boldsymbol{v}} = \boldsymbol{\alpha}_v$ and $\boldsymbol{\lambda} = \boldsymbol{f}_\lambda$. The respective joint torque control component derived via (11) is

$$\begin{aligned} \boldsymbol{\tau}_p &= \boldsymbol{M}_{Al}^T \boldsymbol{S}_v \boldsymbol{\alpha}_v + \boldsymbol{M}_l \ddot{\boldsymbol{\theta}}_p^{ref} - \boldsymbol{J}^T \mathcal{F}_B + \boldsymbol{c}_l + \boldsymbol{g}_l \\ &= \left(\boldsymbol{M}_{Al}^T - \boldsymbol{M}_l \boldsymbol{M}_{Al}^{+} \boldsymbol{M}_A\right) \boldsymbol{S}_v \boldsymbol{\alpha}_v + \boldsymbol{M}_l \boldsymbol{M}_{Al}^{+} \boldsymbol{S}_f \boldsymbol{f}_\lambda \\ &\quad + \left(\boldsymbol{M}_l \boldsymbol{M}_{Al}^{+} \boldsymbol{T} - \boldsymbol{J}^T\right) \mathcal{F}_B \\ &\quad + \boldsymbol{c}_l + \boldsymbol{g}_l - \boldsymbol{M}_l \boldsymbol{M}_{Al}^{+}\left(\mathcal{C}_A + \mathcal{G}_A + \boldsymbol{M}_A \dot{\boldsymbol{S}}_v \boldsymbol{v}\right). \end{aligned} \tag{33}$$

This control torque compensates the joint-space non-linear and gravity forces and ensures a double-integrator type closed-loop behavior $\ddot{\boldsymbol{\theta}} = \ddot{\boldsymbol{\theta}}_p^{ref}$. When compared to the particular-solution control torque derived under the OS formulation, $\boldsymbol{\tau} = \boldsymbol{J}^T(\boldsymbol{\theta})\mathcal{F}^{ref}$, $\mathcal{F}^{ref}$ given in (5), the above expression is somewhat messier. But we can expect a better nominal behavior in joint-space, as explained. The following remarks are due. First, note that with the controller we have to compensate the exact non-linear force term $\mathcal{C}_A$ instead of compensating its approximation $\mathcal{C}_A \approx \dot{\boldsymbol{M}}_A \mathcal{V}_A + \dot{\boldsymbol{M}}_{Al}\dot{\boldsymbol{\theta}}$ that was required for momentum conservation (19); otherwise, the task-space behavior cannot be guaranteed

https://doi.org/10.1017/S0263574715000466 Published online by Cambridge University Press

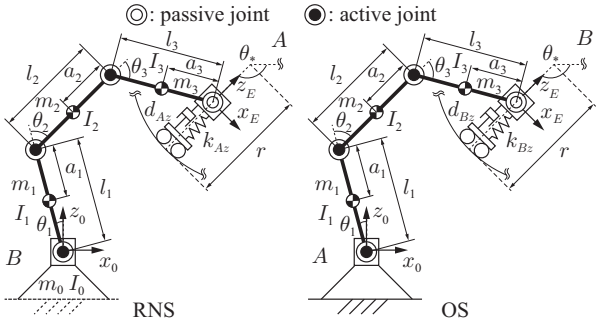


Fig. 3. Planar five-link four-joint manipulator models used in the RNS and OS formulations. The "root" links are end-links A (for RNS this is the end effector, while for OS this is the base). The passive joints at the two end effectors appear since end-effector orientation is ignored. The "fixed-base" link B in the RNS formulation is obtained by a constraint force calculated via the Lagrange multiplier method.

anymore. The integrability property will deteriorate in that case only insignificantly, as will be shown below with the simulation. Second, note that, on the other hand, the integrability property depends very much on the null-space (reactionless) acceleration (21) (cf. Corollary 1). Since the controller (33) is solely based on a particular-solution component, the desirable joint-acceleration integrability will be compromised to some extend and hence, there will be some residual joint-velocity drift. Because of the momentum conservation property, however, this drift is expected to be substantially smaller than that of a similar OS controller. Third, if integrability is the only secondary task envisioned, then the reactionless acceleration (21) should be added as a control component.

5. A Comparative Study

Motion/force control under the OS formulation[4,9] and the newly introduced EE-RNS formulation will be compared herein. Starting with the floating-base model, we constrain end-link B via $\mathcal{F}_B$, calculated with the help of the Lagrange multiplier method. The kinetic energy term for end-link B (the last term in (27)) is zero, hence (28) becomes

$$T = \frac{1}{2}\mathcal{V}_A^T \tilde{\boldsymbol{M}}_A \mathcal{V}_A + \frac{1}{2}\dot{\boldsymbol{\theta}}^T \tilde{\boldsymbol{M}}_l \dot{\boldsymbol{\theta}} + \mathcal{V}_A^T \tilde{\boldsymbol{M}}_{Al} \dot{\boldsymbol{\theta}}, \tag{34}$$

where the tilde operator denotes inertia matrices modified to account for the constraint acting on end-link B. This notation will be used below in all floating-base relations derived so far.

5.1. Models

Two equivalent planar five-link four R-joint manipulator models will be employed as shown in Fig. 3. The only difference is in the assignment of root link A as end-effector or base in the RNS and OS formulations, respectively. All link parameters are identical: link mass, inertia, length and CoM position are set to $m_j = 10$ kg, $I_j = 0.83$ kgm^2, $l_j = 1.0$ m, $a_j = 0.5$ m ($j = 1, 2, 3$), respectively. The base-link parameters in the RNS formulation are set at $m_0 = 10^4$ kg and $I_0 = 830$ kgm^2 (the link length is irrelevant). Note, the base link is constrained but nevertheless, its parameters determine the joints-space behavior to a great extent. Further on, there is one virtual passive joint at each of the end effectors, such that the respective rotational coordinate can be ignored. Thus, we obtain two equivalent 3R redundant manipulators, with $n = 3$ and two end-effector coordinates (for translational motion only). The end effectors move along a semi-circular surface of radius $r = 0.5$ m. A spring/damper system is attached at each end effector, pointing always along the normal of the circular surface. With this system, positioning/force errors in the constrained direction will be modeled. The spring and damper constants in both models are the same: 5.0×10^4 N/m and 5.0×10^2 Ns/m, respectively.

5.2. Controllers

The performance of the following two motion/force controllers will be examined: the RNS formulation based controller, or RNS-C for short and the OS formulation based controller, or OS-C for short.

https://doi.org/10.1017/S0263574715000466 Published online by Cambridge University Press

Thereby, the main focus is on the task-space (or particular-solution) control component that ensures the nominal behavior in joint space. With RNS-C, control torque (33) will be used; with OS-C — $\boldsymbol{\tau} = \boldsymbol{J}^T \mathcal{F}^{ref}$, $\mathcal{F}^{ref}$ given in (5). The feedback control loops for motion along x direction and force along z direction are designed as

$$\dot{v}_i^{ref} = \dot{v}_i^{des} + k_d(v_i^{des} - v_i) + k_p(x_i^{des} - x_i), \tag{35}$$

$$f_i^{ref} = f_i^{des} + k_f(f_i^{des} - f_i), \tag{36}$$

where k_d, k_p and k_f are feedback gains. In the case of RNS-C ($i = A$), $\dot{v}_A^{ref}$ and f_A^{ref} are to be used in (33) in place of $\boldsymbol{S}_v \boldsymbol{\alpha}_v$ and $\boldsymbol{S}_f \boldsymbol{f}_\lambda$, respectively. In the case of OS-C ($i = B$), on the other hand, $\dot{v}_B^{ref}$ and f_B^{ref} should replace the reference acceleration and the reference contact force appearing in (5) as $\boldsymbol{S}\dot{\mathcal{V}}^{ref}$ and $\boldsymbol{S}^\perp \mathcal{F}_\kappa^{ref}$, respectively.

Further on, to assess the property of dynamic decoupling, null-space control components will be added to the above particular components in the form of null-space joint-motion dampers. The role of null-space component (21) for improving integrability, and hence, for reducing the residual joint velocity, will be also examined.

5.3. Simulation results

Results from two simulations will be presented. Sampling and simulation times are set to 1 ms and 6 s, respectively. Without loss of generality, the gravity term is excluded to keep the focus on dynamic and reactive forces only[3]. The initial configurations in the simulations are the same: $\boldsymbol{\theta} = [-15\ 60\ 60]^T$ deg.

The first simulation uses the particular-solution control torque only (no null-space motion whatsoever). The desired path in the unconstrained direction is defined via a fifth-order spline function, s.t. the end effector tracks a circular arc of $\pm 45^\circ$ in both directions (one full cycle). At the half-cycle, the boundary conditions for the two splines are stationary, such that the end effector pauses instantaneously. The motion feedback gains are set at $k_d = 10\ \text{s}^{-1}$ and $k_p = 100\ \text{s}^{-2}$. The desired force in the constrained direction is designed as a fifth-order spline function during the first second, with a maximum value set at 10 N, to be kept constant for the remaining time. The respective feedback gain is set at $k_f = 5$. Note that the setting of the feedback gains is not critical due to the stability properties of the controllers, stemming from complete dynamic decoupling and reactionless motion for OS-C and RNS-C, respectively. The above values were selected empirically to yield minimal position/force tracking errors.

The second simulation involves null-space motion initialized with a non-zero null-space joint velocity, whereby the initial (stationary) state of the end effector is to be tracked under motion/force feedback control. This results mainly in self-motion.

5.3.1. Particular-solution control torque with pseudoinverse. Figures 4 and 5 show the task and joint-space simulation results obtained with RNS-C and OS-C. From Fig. 4, it is apparent that the end-effector position/force data are almost identical for the two controllers. This means that the properties of full motion/force decoupling could be validated with both controllers. Note that the end-effector position errors in the z direction are larger. These errors are due to the elastic environment modeled via the springs and the lack of position feedback control (pure force control) in this direction.

Further on, from the joint-space behavior results shown in Fig. 5, it becomes apparent that the joint velocity obtained from the OS-C simulation undergoes much larger fluctuations than that in the RNS-C one; the respective peak values are 4.22 rad/s against 0.73 rad/s. This considerably different joint-space behavior can be explained with the condition number of the mobility tensor[4], as shown in Fig. 6. For both controllers, the maximum value is attained around the end of the half-cycle, when the manipulator is mostly extended. The maximum value under OS control, however, is much larger than that under RNS control. Note also that under OS-C, the condition number fluctuates significantly: local peaks can be observed, and in addition, the *rate of change* is also considerably higher than that under RNS-C. These observations show that, indeed, the ill-conditioning of the end-effector mobility

[3] The gravity term is assumed to be fully compensated in the controller (32).
[4] The inverse of this matrix is used only in the OS controller.

https://doi.org/10.1017/S0263574715000466 Published online by Cambridge University Press

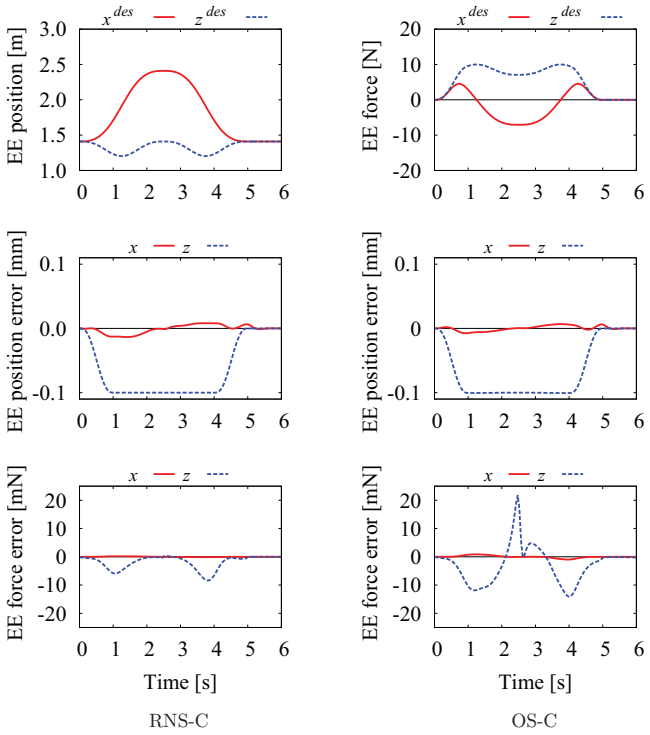


Fig. 4. Simulation results of end-effector position and force obtained with particular-solution control torque only, no null-space component.

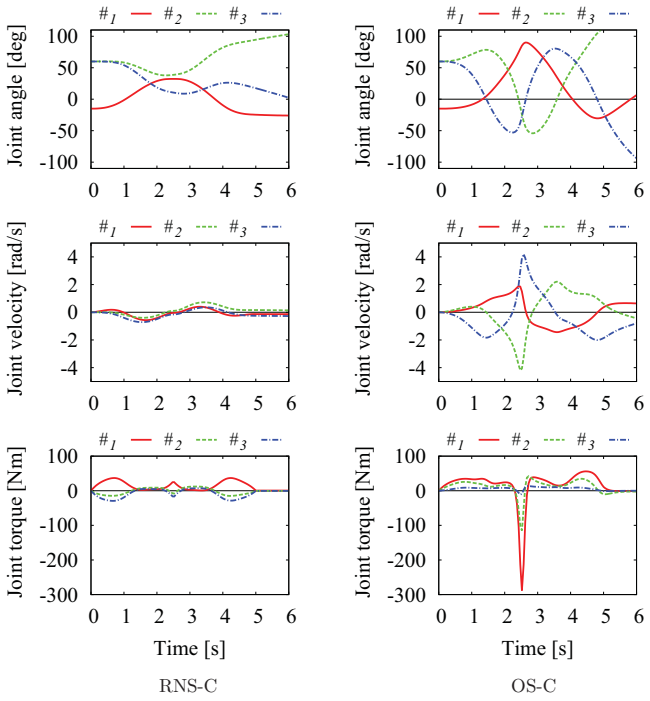


Fig. 5. Simulation results of the joint variables obtained with particular-solution control torque only, no null-space component.

https://doi.org/10.1017/S0263574715000466 Published online by Cambridge University Press

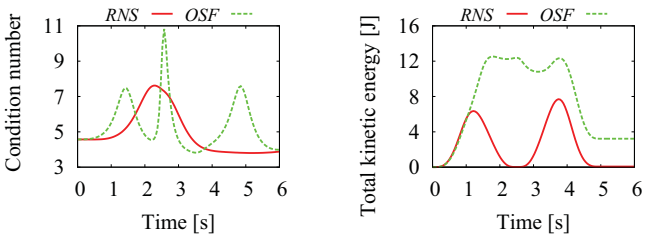


Fig. 6. Performance evaluation criteria obtained with particular-solution control torque only, no null-space component.

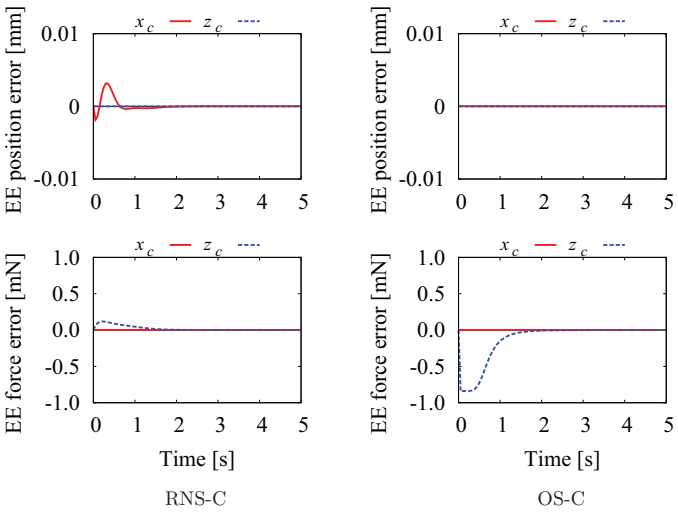


Fig. 7. Simulation results of position and force errors including null-space damping control. In this simulation, end-effector position and force are regulated to their initial values: [1.41 1.41] m for position and null for force.

tensor may influence joint-space behavior to a great extent, as also suggested in other works. As a consequence from the large joint velocity peaks under OS control, joint torque peaks appear, as apparent from Fig. 5. Also, a larger end-effector force error is induced, as seen in Fig. 4.

The joint acceleration near-integrability property of the RNS controller can be assessed via the joint-space velocities shown in Fig. 5. At the half-cycle, when the end-effector pauses to reverse direction, the joint velocities also become almost null, as expected from the momentum conservation condition. This is in contrast to the behavior under OS control: joint velocity peaks are observed for the above-mentioned end-effector state. These peaks are induced via the conditioning of the transform that enforces the dynamically consistent relationship, as explained above. Note also the relatively large residual joint-velocity norm for OS-C at the end of the cycle: 0.87604 rad/s versus the significantly smaller 0.2616 rad/s for RNS-C. Further on, when the reactionless null-space component (21) is employed in addition to the particular one, the residual velocity decreases dramatically to the order of 10^{-4} rad/s.

From Fig. 6, it is seen that the RNS-C outperformed OS-C also in terms of total kinetic energy, in spite of the (local) minimization property of the inertia-weighted generalized inverse. Note that at the end of the half-cycle, the total kinetic energy under RNS-C decreases to zero, in agreement with the condition that generalized momentum is conserved at zero. In contrast, the kinetic energy under OS-C remains at a high level at that point.

5.3.2. Particular plus null-space control torque. The aim of this simulation is to demonstrate the differences in the complete dynamic decoupling property between the particular and the null-space components. In both controllers, null-space motion is initialized via a joint velocity from within the null-space of the Jacobian: $(\boldsymbol{I} - \boldsymbol{J}^{+}\boldsymbol{J})\dot{\boldsymbol{\theta}}_a$, with $\dot{\boldsymbol{\theta}}_a = [10\,10\,10]^T$ rad/s. This joint velocity is then to be damped out with the null-space terms, using $\boldsymbol{\tau}_{RL}$ with $\ddot{\boldsymbol{\theta}}_a = -\boldsymbol{K}_{jd}\dot{\boldsymbol{\theta}}$ for RNS-C (see (23)), and $\boldsymbol{\tau}_a = -\boldsymbol{M}_l\boldsymbol{K}_{jd}\dot{\boldsymbol{\theta}}$ for OS-C (see (6)). The identity matrix is used as the joint damping matrix $\boldsymbol{K}_{jd}$.

https://doi.org/10.1017/S0263574715000466 Published online by Cambridge University Press

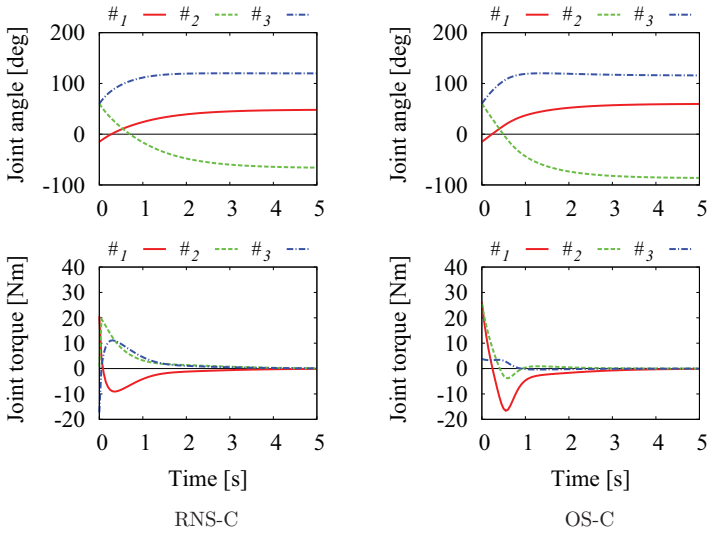


Fig. 8. Simulation results of the joint variables for the case with null-space damping control.

The position of each end effector is regulated thereby to the initial value of [1.41 1.41] m while the force component is regulated to zero. The results are shown in Figs. 7 and 8 for the task-space and joint-space behavior, respectively. First, from Fig. 7 it is seen that with the OS-C, the null-space motion did not affect the end-effector position regulator. This can be explained with the complete dynamic decoupling property of this controller. In the RNS-C case, however, an end-effector error in the position is observed. This situation was anticipated, though, because the controller does not ensure exact complete dynamic decoupling. Nevertheless, as seen from the results, the RNS controller performs well, which can be attributed to the reactionless motion property.

6. Conclusions and Discussion

The contribution of this work is the development of a framework for task-space dynamics and its application to motion/force control. The aim was to address the not yet fully understood problematic joint-space behavior of redundant robots exhibiting otherwise satisfactory performance in task-space under motion/force or impedance control. We assumed that the problem was caused by two conditions: (i) ill-conditioning of the inverse link-inertia matrix appearing in the end-effector mobility tensor, and (ii) joint velocity residual due to non-integrability of joint acceleration. It was shown that these problems can be tackled with the help of the RNS method used in previous works to minimize base reactions of free-floating and flexible-base robots. The main characteristics of the method are joint-space decomposition via the coupling inertia matrix and its momentum conservation ability, which are essential in generating reactionless motions. A dynamically consistent force/torque relation for complete dynamic decoupling was derived with a weighted generalized inverse of the coupling inertia matrix, wherein the inverse link inertia was used as the weight matrix. This type of generalized inverse has a similar structure as the dynamically consistent inverse in the OS formulation; both inverses are prone to ill-conditioning. The problem cannot be alleviated under the OS formulation, unless the null-space dynamics are involved. This, however, means that the null-space dynamics may become unavailable for other subtasks. On the other hand, as shown herein, under the RNS formulation it is possible to address ill-conditioning by employing the pseudoinverse of the coupling inertia matrix, and without resorting to the null-space dynamics. The complete dynamic decoupling property diminishes, but the reactionless motion property is preserved, as a necessary condition for the decoupling.

Further on, the necessary and sufficient conditions for integrability were identified in relation to momentum conservation. Under the motion/force control scenario with a fixed-base robot discussed herein, external forces are present and therefore, the necessary condition for integrability cannot be met exactly. Nevertheless, simulation experiments have shown that the proposed RNS-based redundancy resolution approach has the potential of reducing the residual joint velocity. It must be

https://doi.org/10.1017/S0263574715000466 Published online by Cambridge University Press

noted that the mass distribution in the system determines the joint-space behavior to a great extent. Especially, the mass of the base link that was constrained via the Lagrange multiplier method, plays an important role. When the mass approaches infinity, the behavior of the manipulator in joint-space coordinates comes close to the one under resolved-acceleration control.[39] As a consequence, our RNS motion/force controller exhibits the behavior of a resolved-acceleration controller in joint space.

The performance of the RNS motion/force controller was investigated via simulations with a planar robot arm, focusing mainly on the particular-solution component. Results from a comparison with an OS motion/force controller have confirmed that position- and force-tracking errors were of the same order. The RNS controller, however, exhibited a significantly better performance in terms of joint-space motion: it was possible to avoid the excessive joint velocity and torque peaks of the OS controller. Also, the residual joint-velocity build-up after a cyclic motion was less than that of the OS controller. The total kinetic energy was also lower, which was attributed to the local minimization property of the coupling kinetic energy exchanged between the end effector and the rest of the links. On the other hand, when a null-space control component was added, the performance of the RNS controller deteriorated somewhat. This was due to the trade-off in the RNS controller design wherein the complete dynamic decoupling property between the task and null-space dynamics was sacrificed in lieu of better joint-space behavior. As was shown in Corollary 1, the null-space component is important for the integrability. Therefore, these trade-offs need to be examined further in a future work.

With regard to practical implementations, it should be noted that in general, model uncertainties will lead to performance deterioration in both controllers. The deterioration will be stronger for the OS controller, though, since the underlying transform (or metric) is prone to ill-conditioning, as explained already above. Further on, most practical implementations would involve a spatial manipulator rather than the planar one discussed here. The momentum of a spatial manipulator includes an angular component, in addition to the linear one investigated here. This may lead to deterioration in the near-integrability property of the RNS controller.

Finally, it is important to note that the reaction forces are explicitly available as a byproduct of the floating-base formulation. These forces are irrelevant in the case of a fixed-base manipulator. But for floating-base robots (on a mobile or flexible base, humanoids and so on), these forces play an important role. We believe that the potential of the RNS motion/force controller is exactly in this field. We intend to confirm this in the near future.

Acknowledgments

The involvement of Dr Naoyuki Hara at the initial stage of the research is acknowledged. The anonymous reviewers raised some important issues that were helpful to improve the manuscript.

References

1. A. Balestrino, G. De Maria and L. Sciavicco, "Adaptive Control of Manipulators in the Task Oriented Space," *Proceedings 13th International Symposim Industrial Robots*, Chicago, IL, (1983) pp. 131–146.
2. N. Hogan, "Impedance control: An approach to manipulation: Part II-implementation," *J. Dyn. Syst. Meas. Control* **107**(1), 8 (1985). Available at: `http://link.aip.org/link/JDSMAA/v107/i1/p8/s1&Agg=doi`
3. S. Hayati, "Hybrid Position/Force Control of Multi-Arm Cooperating Robots," *Proceedings IEEE International Conference on Robotics and Automation*, San Francisco, CA (1986) pp. 82–89. Available at: `http://ieeexplore.ieee.org/lpdocs/epic03/wrapper.htm?arnumber=1087650`
4. O. Khatib, "A unified approach for motion and force control of robot manipulators: The operational space formulation," *IEEE J. Robot. Autom.* **3**(1), 43–53 (Feb. 1987). Available at: `http://ieeexplore.ieee.org/lpdocs/epic03/wrapper.htm?arnumber=1087068`
5. L. Villani and J. De Schutter, "Force Control," **In**: *Springer Handbook of Robotics* (B. Siciliano and O. Khatib, eds.) (Berlin, Heidelberg: Springer Verlag, 2008) ch. 7, pp. 161–186. Available at: `http://www.springerlink.com/index/10.1007/978-3-540-30301-5`
6. P. Hsu, J. Hauser and S. Sastry, "Dynamic Control of Redundant Manipulators," *Proceedings IEEE International Conference on Robotics and Automation*, IEEE Comput. Soc. Press, Philadelphia, PA, no. 6. (1988) pp. 183–187. Available at: `http://ieeexplore.ieee.org/lpdocs/epic03/wrapper.htm?arnumber=12045`
7. W. Newman and M. Dohring, "Augmented Impedance Control: An Approach to Compliant Control of Kinematically Redundant Manipulators," *Proceedings IEEE International Conference on Robotics*

https://doi.org/10.1017/S0263574715000466 Published online by Cambridge University Press

and Automation, no. April, IEEE Comput. Soc. Press, Sacramento, CA (1991) pp. 30–35. Available at: http://ieeexplore.ieee.org/lpdocs/epic03/wrapper.htm?arnumber=131548
8. Z.-X. Peng and N. Adachi, "Compliant motion control of kinematically redundant manipulators," *IEEE Trans. Robot. Autom.* **9**(6), 831–836 (1993). Available at: http://ieeexplore.ieee.org/lpdocs/epic03/wrapper.htm?arnumber=265926
9. O. Khatib, "Inertial properties in robotic manipulation: An object-level framework," *Int. J. Robot. Res.* **14**(1), 19–36 (1995). Available at: http://ijr.sagepub.com/cgi/doi/10.1177/027836499501400103
10. R. Featherstone and O. Khatib, "Load independence of the dynamically consistent inverse of the Jacobian matrix," *Int. J. Robot. Res.* **16**(2), 168–170 (Apr. 1997). Available at: http://ijr.sagepub.com/cgi/doi/10.1177/027836499701600203
11. J. Baillieul, "Kinematic Programming Alternatives for Redundant Manipulators," *Proceedings IEEE International Conference on Robotics and Automation*, St. Louis, MO (1985) pp. 722–728. Available at: http://ieeexplore.ieee.org/lpdocs/epic03/wrapper.htm?arnumber=1087234
12. J. Park, W. Chung and Y. Youm, "On Dynamical Decoupling of Kinematically Redundant Manipulators," *Proceedings IEEE/RSJ International Conference on Intelligent Robots and Systems*, Kyongju, Korea, vol. 3 (1999) pp. 1495–1500. Available at: http://ieeexplore.ieee.org/lpdocs/epic03/wrapper.htm?arnumber=811690
13. K. C. Park, P.-H. Chang and S. Lee, "Analysis and control of redundant manipulator dynamics based on an extended operational space," *Robotica* **19**(06), 649–662 (2001). Available at: http://www.journals.cambridge.org/abstract_S0263574701003599
14. C. Ott, A. Kugi and Y. Nakamura, "Resolving the Problem of Non-Integrability of Nullspace Velocities for Compliance Control of Redundant Manipulators by using Semi-Definite Lyapunov Functions," *Proceedings IEEE International Conference on Robotics and Automation*, Pasadena, CA (May 2008) pp. 1999–2004. Available at: http://ieeexplore.ieee.org/lpdocs/epic03/wrapper.htm?arnumber=4543500
15. C. Natale, B. Siciliano and L. Villani, "Spatial Impedance Control of Redundant Manipulators," *Proceedings IEEE International Conference on Robotics and Automation*, Detroit, MI, vol. 3 (May, 1999) pp. 1788–1793. Available at: http://ieeexplore.ieee.org/lpdocs/epic03/wrapper.htm?arnumber=770368
16. B. Nemec and L. Zlajpah, "Null space velocity control with dynamically consistent pseudo-inverse," *Robotica* **18**(5), 513–518 (Sep. 2000). Available at: http://www.journals.cambridge.org/abstract_S0263574700002800
17. A. Albu-Schaffer, C. Ott, U. Frese and G. Hirzinger, "Cartesian Impedance Control of Redundant Robots: Recent Results with the DLR-Light-Weight-Arms," *Proceedings IEEE International Conference of Robotics and Automation*, Taipei, Taiwan, vol. 3 (2003) pp. 3704–3709. Available at: http://ieeexplore.ieee.org/xpl/login.jsp?tp=&arnumber=1242165&url=http%3A%2F%2Fieeexplore.ieee.org%2Fxpls%2Fabs_all.jsp%3Farnumber%3D1242165
18. J. Peters, M. Mistry, F. Udwadia, J. Nakanishi and S. Schaal, "A unifying framework for robot control with redundant DOFs," *Auton. Robots* **24**(1), 1–12 (Oct. 2008). Available at: http://link.springer.com/10.1007/s10514-007-9051-x
19. N. Hogan, "Impedance Control: An Approach to Manipulation," *Proceedings American Control Conference*, San Diego, CA (1984) pp. 304–313.
20. K.-S. Chang and O. Khatib, "Efficient Algorithm for Extended Operational Space Inertia Matrix," *Proceedings IEEE/RSJ International Conference on Intelligent Robots and Systems*, Kyongju, Korea, vol. 1 (1999) pp. 350–355. Available at: http://ieeexplore.ieee.org/lpdocs/epic03/wrapper.htm?arnumber=813028
21. T. Yoshikawa, "Manipulability of robotic mechanisms," *Int. J. Robot. Res.* **4**(2), 3–9 (Jun. 1985). Available at: http://ijr.sagepub.com/content/4/2/3.full.pdf+html
22. J. Nakanishi, R. Cory, M. Mistry, J. Peters and S. Schaal, "Operational space control: A theoretical and empirical comparison," *Int. J. Robot. Res.* **27**(6), 737–757 (Jun. 2008). Available at: http://ijr.sagepub.com/cgi/doi/10.1177/0278364908091463
23. J. Hollerbach, "Redundancy resolution of manipulators through torque optimization," *IEEE J. Robot. Autom.* **3**(4), 308–316 (Aug. 1987). Available at: http://ieeexplore.ieee.org/lpdocs/epic03/wrapper.htm?arnumber=1087111
24. S. Ma, S. Hirose and D. N. Nenchev, "Improving local torque optimization techniques for redundant robotic mechanisms," *J. Robot. Syst.* **8**(1), 75–91 (Feb. 1991). Available at: http://doi.wiley.com/10.1002/rob.4620080106
25. G. Oriolo and Y. Nakamura, "Free-Joint Manipulators: Motion Control Under Second-Order Nonholonomic Constraints," *Proceedings IEEE/RSJ International Workshop on Intelligent Robots and Systems*, Osaka, Japan (1991) pp. 1248–1253. Available at: http://ieeexplore.ieee.org/lpdocs/epic03/wrapper.htm?arnumber=174671
26. S. Ma and D. N. Nenchev, "Local torque minimization for redundant manipulators: A correct formulation," *Robotica* **14**(2), 235–239 (Mar. 1996). Available at: http://journals.cambridge.org/abstract_S0263574700019159
27. K. O'Neil, "Divergence of linear acceleration-based redundancy resolution schemes," *IEEE Trans. Robot. Autom.* **18**(4), 625–631 (Aug. 2002). Available at: http://ieeexplore.ieee.org/lpdocs/epic03/wrapper.htm?arnumber=1044375

https://doi.org/10.1017/S0263574715000466 Published online by Cambridge University Press

28. A. Bowling and S. Harmeyer, "Repeatable redundant manipulator control using nullspace quasivelocities," *J. Dyn. Syst. Meas. Control* **132**(3), 031007 (2010). Available at: http://link.aip.org/link/JDSMAA/v132/i3/p031007/s1&Agg=doi
29. H. Sadeghian, L. Villani, M. Keshmiri and B. Siciliano, "Dynamic multi-priority control in redundant robotic systems," *Robotica* **31**, 1–13 (May 2013). Available at: http://www.journals.cambridge.org/abstract_S0263574713000416
30. M. Cefalo, G. Oriolo and M. Vendittelli, "Planning Safe Cyclic Motions Under Repetitive Task Constraints," *Proceedings IEEE International Conference on Robotics and Automation*, Karlsruhe, Germany (May 2013) pp. 3807–3812. Available at: http://ieeexplore.ieee.org/lpdocs/epic03/wrapper.htm?arnumber=6631112
31. Y. Zhang, D. Guo and S. Ma, "Different-level simultaneous minimization of joint-velocity and joint-torque for redundant robot manipulators," *J. Intell. Robot. Syst.* **72**(3–4), 301–323 (Mar. 2013). Available at: http://link.springer.com/10.1007/s10846-013-9816-8
32. D. Nenchev, K. Yoshida and M. Uchiyama, "Reaction Null-Space Based Control of Flexible Structure Mounted Manipulator Systems," *Proceedings of 35th IEEE Conference on Decision and Control*, Kobe, Japan (1996) pp. 4118–4123. Available at: http://ieeexplore.ieee.org/lpdocs/epic03/wrapper.htm?arnumber=577417
33. K. Yoshida and D. Nenchev, "Moving Base Robotics and Reaction Management Control," *Robotics Research: The 7th International Symposium* (G. Giralt and G. Hirzinger, ed.) (Springer Verlag, Herrsching, Germany, 1996) pp. 101–109. Available at: http://link.springer.com/chapter/10.1007\%2F978-1-4471-0765-1_11
34. D. Nenchev, K. Yoshida and Y. Umetani, "Introduction of Redundant Arms for Manipulation in Space," *IEEE/RSJ International Workshop on Intelligent Robots*, Tokyo, Japan (1988) pp. 679–684. Available at: http://ieeexplore.ieee.org/lpdocs/epic03/wrapper.htm?arnumber=593682
35. A. Gouo, D. Nenchev, K. Yoshida and M. Uchiyama, "Motion control of dual-arm long-reach manipulators," *Adv. Robot.* **13**(6), 617–631 (Jan. 1998). Available at: http://www.tandfonline.com/doi/abs/10.1163/156855399X01846
36. D. Nenchev, K. Yoshida, P. Vichitkulsawat and M. Uchiyama, "Reaction null-space control of flexible structure mounted manipulator systems," *IEEE Trans. Robot. Autom.* **15**(6), 1011–1023 (Dec. 1999). Available at: http://ieeexplore.ieee.org/lpdocs/epic03/wrapper.htm?arnumber=817666
37. S. Abiko, R. Lampariello and G. Hirzinger, "Impedance Control for a Free-Floating Robot in the Grasping of a Tumbling Target with Parameter Uncertainty," *Proceedings IEEE/RSJ International Conference on Intelligent Robots and Systems*, Beijing, China (Oct. 2006) pp. 1020–1025. Available at: http://ieeexplore.ieee.org/lpdocs/epic03/wrapper.htm?arnumber=4058497
38. N. Hara, Y. Handa and D. Nenchev, "End-Link Dynamics of Redundant Robotic Limbs: The Reaction Null Space Approach," *Proceedings IEEE International Conference on Robotics and Automation*, Saint Paul, MN (May 2012) pp. 299–304. Available at: http://ieeexplore.ieee.org/lpdocs/epic03/wrapper.htm?arnumber=6224627
39. J. Luh, M. Walker and R. Paul, "Resolved-acceleration control of mechanical manipulators," *IEEE Trans. Autom. Control* **25**(3), 468–474 (Jun. 1980). Available at: http://ieeexplore.ieee.org/xpls/abs_all.jsp?arnumber=1102367

Appendix A

Closed-loop stability for the motion/force controller in task-space can be inferred from the following derivations. The notations introduced in the beginning of Section 4 are used.

The end-effector motion constraint is

$$\boldsymbol{J}_{\kappa A}\dot{\mathcal{V}}_A + \dot{\boldsymbol{J}}_{\kappa A}\mathcal{V}_A = \boldsymbol{0}. \tag{37}$$

Therefore, (10) can be rewritten as

$$\boldsymbol{M}_A\dot{\mathcal{V}}_A + \boldsymbol{M}_{Al}\ddot{\boldsymbol{\theta}} + \mathcal{C}_A + \mathcal{G}_A = \boldsymbol{J}_{\kappa A}^T\boldsymbol{\lambda} + \boldsymbol{T}\mathcal{F}_B. \tag{38}$$

Combining these two equations, we obtain

$$\boldsymbol{J}_{\kappa A}\boldsymbol{M}_A^{-1}\boldsymbol{J}_{\kappa A}^T\boldsymbol{\lambda} = -\boldsymbol{J}_{\kappa A}\boldsymbol{M}_A^{-1}(\boldsymbol{T}\mathcal{F}_B - \boldsymbol{M}_{Al}\ddot{\boldsymbol{\theta}} - \mathcal{C}_A - \mathcal{G}_A) - \dot{\boldsymbol{J}}_{\kappa A}\mathcal{V}_A \tag{39}$$

and hence,

$$\boldsymbol{\lambda} = \boldsymbol{\Lambda}_f^{-1}\left(\boldsymbol{J}_{\kappa A}\boldsymbol{M}_A^{-1}(\boldsymbol{M}_{Al}\ddot{\boldsymbol{\theta}} + \mathcal{C}_A + \mathcal{G}_A - \boldsymbol{T}\mathcal{F}_B) - \dot{\boldsymbol{J}}_{\kappa A}\mathcal{V}_A\right), \tag{40}$$

https://doi.org/10.1017/S0263574715000466 Published online by Cambridge University Press

where $\boldsymbol{\Lambda}_f \equiv \boldsymbol{J}_{\kappa A}\boldsymbol{M}_A^{-1}\boldsymbol{J}_{\kappa A}^T$. Then, substitute $\boldsymbol{\lambda}$ into (38) to obtain

$$\boldsymbol{M}_A\dot{\mathcal{V}}_A + \boldsymbol{J}_{\kappa A}^T\boldsymbol{\Lambda}_f^{-1}\dot{\boldsymbol{J}}_{\kappa A}\mathcal{V}_A = -\boldsymbol{P}(\boldsymbol{M}_{Al}\ddot{\boldsymbol{\theta}} + \mathcal{C}_A + \mathcal{G}_A - \boldsymbol{T}\mathcal{F}_B), \tag{41}$$

where $\boldsymbol{P} = \boldsymbol{I} - \boldsymbol{J}_{\kappa A}^T\boldsymbol{\Lambda}_f\dot{\boldsymbol{J}}_{\kappa A}\boldsymbol{M}_A^{-1}$ and $\boldsymbol{P}\boldsymbol{J}_{\kappa A}^T = \boldsymbol{0}$. Next, by multiplying both sides of (41) with $\boldsymbol{S}_v^T$ from the left and using $\boldsymbol{S}_v^T\boldsymbol{P} = \boldsymbol{S}_v^T$ and $\dot{\mathcal{V}}_A = \boldsymbol{S}_v\dot{\boldsymbol{\nu}} + \dot{\boldsymbol{S}}_v\boldsymbol{\nu}$, we obtain

$$\boldsymbol{S}_v^T\boldsymbol{M}_A\boldsymbol{S}_v\dot{\boldsymbol{\nu}} + \boldsymbol{S}_v^T\boldsymbol{M}_A\dot{\boldsymbol{S}}_v\boldsymbol{\nu} = -\boldsymbol{S}_v^T(\boldsymbol{M}_{Al}\ddot{\boldsymbol{\theta}} + \mathcal{C}_A + \mathcal{G}_A - \boldsymbol{T}\mathcal{F}_B) \tag{42}$$

or

$$\boldsymbol{\Lambda}_v\dot{\boldsymbol{\nu}} = -\boldsymbol{S}_v^T(\boldsymbol{M}_{Al}\ddot{\boldsymbol{\theta}} + \mathcal{C}_A + \mathcal{G}_A - \boldsymbol{T}\mathcal{F}_B + \boldsymbol{M}_A\dot{\boldsymbol{S}}_v\boldsymbol{\nu}), \tag{43}$$

where $\boldsymbol{\Lambda}_v \equiv \boldsymbol{S}_v^T\boldsymbol{M}_A\boldsymbol{S}_v$. Further on, noting that $\dot{\boldsymbol{S}}_f^T\boldsymbol{S}_v = -\boldsymbol{S}_f^T\dot{\boldsymbol{S}}_v$, we rewrite (40) as

$$\boldsymbol{\lambda} = \boldsymbol{\Lambda}_f^{-1}\boldsymbol{J}_{\kappa A}\boldsymbol{M}_A^{-1}(\boldsymbol{M}_{Al}\ddot{\boldsymbol{\theta}} + \mathcal{C}_A + \mathcal{G}_A - \boldsymbol{T}\mathcal{F}_B + \boldsymbol{M}_A\dot{\boldsymbol{S}}_v\boldsymbol{\nu}). \tag{44}$$

The control equation:

$$\boldsymbol{M}_{Al}\ddot{\boldsymbol{\theta}} = \boldsymbol{S}_f\boldsymbol{f}_\lambda - \boldsymbol{M}_A\boldsymbol{S}_v\boldsymbol{\alpha}_v - \mathcal{C}_A - \mathcal{G}_A + \boldsymbol{T}\mathcal{F}_B - \boldsymbol{M}_A\dot{\boldsymbol{S}}_v\boldsymbol{\nu} \tag{45}$$

is substituted into (43) and (44) to confirm that the closed-loop relations for motion and force are decoupled as $\dot{\boldsymbol{\nu}} = \boldsymbol{\alpha}_v$ and $\boldsymbol{\lambda} = \boldsymbol{f}_\lambda$, respectively.

https://doi.org/10.1017/S0263574715000466 Published online by Cambridge University Press